ChemComm

Accepted Manuscript

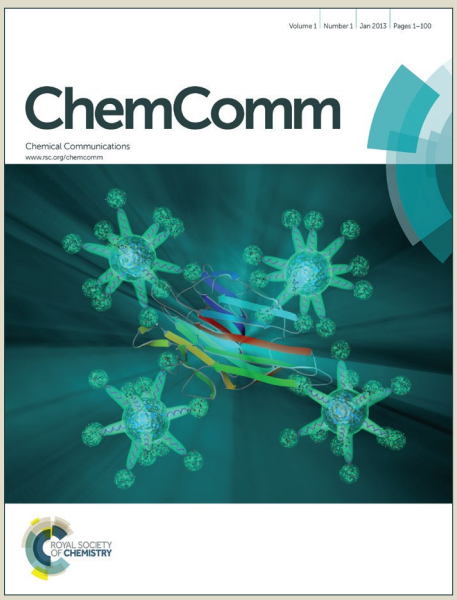

ROYAL SOCIETY OF CHEMISTRY

www.rsc.org/chemcomm

Journal Name

COMMUNICATION

Chemical synthesis of porous hierarchical Ge-Sn binary composite by metathesis reaction for rechargeable Li-ion batteries

Received 00th January 20xx,
Accepted 00th January 20xx

DOI: 10.1039/x0xx00000x

www.rsc.org/

*Ning Lin [a], Jie Zhou [a], Ying Han [a], Kailong Zhang [a], Yongchun Zhu [a] *, and Yitai Qian[a] **

Direct metathesis reaction between Mg_2Ge and $SnCl_4$ is introduced to prepare porous hierarchical Ge-Sn binary composite, in which the Ge and Sn components are distributed uniformly, with a tap density of 2.3 g cm^{-3}. As anode for LIBs, the Ge-Sn composite displays a specific capacity of 980 mAh g^{-1} at 0.5 A g^{-1} after 250 cycles, 890 mAh g^{-1} at 3 A g^{-1} over 1700 cycles. When paired with a commercial $LiCoO_2$ cathode, a 3.6 V full battery with a capacity of 830 mAh g^{-1} is obtained.

Group IV elements including Silicon (Si), Germanium (Ge), and Tin (Sn) are intensively investigated as potential alternative materials to conventional graphite anode in rechargeable Li-ion batteries (LIBs). [1] The theoretical Li^+ storage capacity for Si, Ge, and Sn anodes are of 3579, 1384, and 991 mAh g^{-1}, respectively. Among them, the Ge exhibits fastest Li ion diffusivity which is 4×10^2 and 6×10^3 times faster than that of Si and Sn. The Sn displays best electrical conductivity. [2, 3] However, the main challenge facing those alloy-type anode is the drastic volume change due to a large amount of Li^+ alloy/de-alloy reaction with active materials during cycling, thus leading to rapid capacity fading. [4]

To address this issues, recently, there is a great interesting in constructing binary phase anode such as Si-Ge, Si-Sn, and Ge-Sn due to their advantageous synergistic effects. Notably, the binary composite undergoes a stepwise lithiation/delithiation procedure, which favors for suppressing the huge volume variations. [5, 6] Additionally, the binary composite allows the anode to benefit from dual advantages such as high specific capacity and high electrical/ionic conductivity, associated with a moderate operating voltage. [7-9]

In this regard, various elaborated synthetic routes have been developed to prepare group IV contained binary anode materials. One of them was chemical/physical vapor deposition including decomposing SiH_4 and GeH_4, [6, 8] and high vacuum co-evaporative or sputtering deposition of Si, Ge or Sn. [7, 9-11] The other widely used method was chemical reduction of complex precursors via gaseous/liquid/solid phase reaction such as magnesiothermic reduction of SiO_2/GeO_2 at 650 °C, [12] reduction $SiCl_4$ and $GeCl_4$ with H_2 at 760 °C, [5] reduction of $SnCl_x$ (X=2, 4) and $GeCl_4$ or $SiCl_4$ with sodium naphthalenide in organic solution. [13-15] What' more, direct annealing and mechanical treatment of precursor mixture were also demonstrated by a few reports such as gas-phase laser photolysis reaction of tetramethyl germanium and tetramethyl tin, direct ball milling of Ge_xSi_{1-x}, and melt spinning of Ge and Sn powder. [3, 16-17]

Since great attention has been attracted, designing universally applicable strategy is urgent to further promote the development of binary phase anode. Previously, metathesis reaction was widely utilized for preparing individual group IV element based materials. For example, nanostructured Si were produced from reacting M_xSi (M= Mg, Na, K) with $SiCl_4$ or other chloride. [18-19] nanostructured Ge was also synthesized through reacting Mg_2Ge with germanium tetrachloride ($GeCl_4$). [20] Very recently, our group reported one-step metathesis reaction between Mg_2Si and GeO_2 for synthesizing Si/Ge composite that are generated synchronously. [21]

Inspired by these well-established reaction, herein, the preparation of β-Sn and Ge binary composite (Ge-Sn) is realized through the typical metathesis reaction between solid Mg_2Ge and liquid $SnCl_4$ at 250 °C, $Mg_2Ge + SnCl_4 = Sn + Ge + 2MgCl_2$. The prepared Ge-Sn composite shows porous hierarchical structure in which the interconnected Ge and Sn nanoparticles are distributed uniformly, and the tap density is about 2.3 g cm^{-3}. As anode for LIBs, the as-prepared Ge-Sn composite delivers a reversible capacity of 980 mAh g^{-1} at 0.5 A g^{-1} after 250 cycles, 890 mAh g^{-1} at 3 A g^{-1} over 1700 cycles, and with fine rate capability of 650 mAh g^{-1} even at 20 A g^{-1}. When paired with a commercial $LiCoO_2$ cathode, a 3.6 V full lithium ion battery with a capacity of 830 mAh g^{-1} is obtained. Impressively, the relevant synthetic route was demonstrated to be applicable for fabricating other binary composite, such as nano-sized Si-Sn and Si-C composites via metathesis reaction between Mg_2Si and $SnCl_4$ or CCl_4, respectively.

Figure 1a shows the XRD patterns of the final product. A group of peaks marked as "♦" could be assigned to the cubic phase Ge (JCPDS No. 03-0478), the other peaks are characterized as tetragonal phase β-Sn (JCPDS No. 01-0926). Based on Scherrer

[a] *Department of Chemistry, University of Science and Technology of China, Hefei, Anhui 230026, P. R. China. E-mail: ychzhu@ustc.edu. cn; ytqian@ustc.edu.cn*

† Electronic Supplementary Information (ESI) available: Experimental section; auxiliary analysis such as XRD, Raman, XPS, BET, EDX mapping images of the as-prepared samples. See DOI: 10.1039/x0xx00000x

Equation, the average size of the produced Ge and Sn particles are estimated to be about 20 and 30 nanometers, favoring the uniform mixture. Figure 1b shows the Raman spectrum of the obtained Ge-Sn composite. The sharp peak at around 285 cm^{-1} corresponds to the Ge-Ge vibration, the shift from 300 cm^{-1} for the bulk Ge (Figure S2) to 285 cm^{-1} may be due to the smaller particle size of the prepared Ge. [22] The broad peak observed at 205 cm^{-1} is assigned to the Sn-Ge phonon mode, suggesting spectroscopic evidence for the presence of Sn-Ge coordination and the formation of an extended random $Sn_{1-x}Ge_x$ alloy. [23]

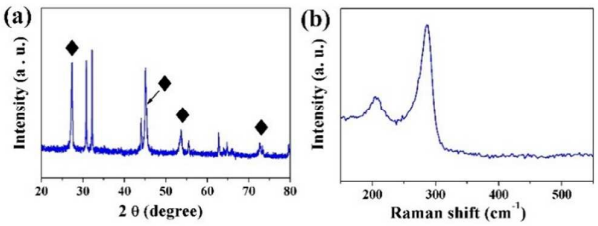

Figure 1 (a) XRD and (b) Raman spectrum of the obtained Ge-Sn product.

The morphology and size of the prepared Ge-Sn product is detected by electron microscopy. The SEM (Figure 2a) shows that the product consists of micro-particles with a size up to a few micron-meters. The enlarged SEM (Figure 2b) and TEM (Figure 2c) images indicate that these particles are constructed by nano-sized particles which are interconnected with each other tightly. The tap density of the sample is measured to be 2.3 g cm^{-3}, which is one advantage of hierarchical structure, favoring high volumetric capacity. [24] Nitrogen adsorption (Brunauer–Emmett–Teller, BET, Figure S3a) measurements indicate that the specific surface area of the Ge-Sn composite is 58.2 m^2 g^{-1}, and the Barrett- Joyner–Halenda (BJH, Figure S3b) analyses of the nitrogen adsorption curves show that the composite possesses a pore volume of 0.17 cm^3 g^{-1}, associated with an average pore size of 34.3 nm. The porous structure may be formed by removing the by-product of $MgCl_2$. To determine the element distribution, the EDX mapping picture is measured, as shown in Figure 2d-f. Clearly, the Ge and Sn elements of the selected irregular particle is distributed uniformly. The other micro-particles is also studied using EDX mapping, as shown in Figure S4, indicating the uniform mixture of Ge and Sn. It is because that the Sn and Ge are generated simultaneously as the proposed reaction proceeding. The element ratio of Ge and Sn are measured to be about 55/45. The X-ray photoelectron spectroscopy (XPS) spectrum (Figure S5) indicates the existence of GeO_x and SnO_x on the surface of the composite, generally formed on the surface during exposure the sample in air. [25] Importantly, this type of metathesis reaction can also be extended to prepare other group IV elements contained binary composite. It is demonstrated that the Si-Sn and Si-C composite are produced through reacting Mg_2Si with $SnCl_4$ and CCl_4 at 230 ^oC, respectively (Figure S6).

The lithium ion storage performance of the as-prepared Ge-Sn composite is first evaluated by the half coin-type cells. The cyclic voltammetry plots with a voltage window between 0.01 and 2.0 V (vs Li/Li^+) are depicted in Figure 3a. In the first cycle, the reduction peak at 1.2 V vs Li/Li^+, which is absent in the subsequent cycle, is attributed to the decomposition of electrolyte and the formation of solid electrolyte interface (SEI) membrane. [13] Below 1.0 V, a series of reduction peaks are related to the Li alloying reaction with Sn-Ge and the formation of multiple Li_xSn and Li_xGe alloys that agrees well with previous report. [13, 14] In the first cathode part, a cascade of oxidation waves are corresponding to the de-alloying reaction of the Ge and Sn based alloys. From second cycle forward, all the plots are overlapped well, implying fine cycling stability.

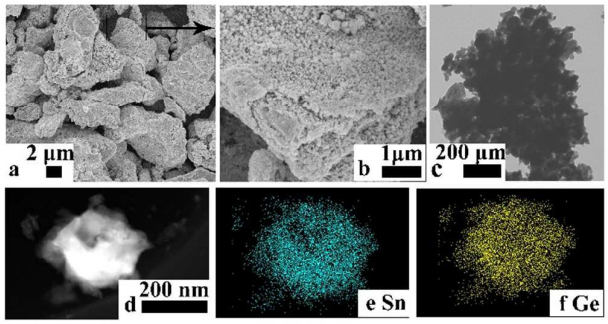

Figure 2. The (a) SEM, (b) enlarged SEM, and (c) TEM images of the prepared Ge-Sn composite. The EDX mapping picture of (e) Sn and (f) Ge elements from the selected particles of (d).

Figure 3b shows the galvanostatic discharge/charge voltage profiles at a current density of 0.3 A g^{-1}. Obviously, Ge-Sn composite undergoes a stepwise lithiation/delithiation process because of the dual-component of Ge and Sn. The initial discharge/charge voltage plots becomes sloping that mainly caused by the phase change from crystalized to amorphous of active component. [14, 17] The initial discharge/charge capacity are 2358.6 and 1811.8 mAh g^{-1}, respectively. The corresponding coulombic efficiency (CE) is 76.8%. The losing of capacity may be caused by the inevitable formation of SEI film and the irreversible reaction between Li^+ and active components such as SnO_x and GeO_x.

Next, the cycling behavior of the Ge-Sn composite is elucidated by galvanostatic discharge/charge test. At a current density of 0.5 A g^{-1}, the Ge-Sn composite delivers a reversible discharge capacity of 980 mAh g^{-1} after 250 cycles (Figure 3c). Apart from the obviously capacity fading of the first three cycles resulted from irreversible Li^+ consumption, the capacity retention is over 75% from third to 250th cycles, with a decaying rate of 0.09%. The CE increases from 76% for the first cycle to 92% for the second cycle, and further up to 98% in the subsequent 250 cycles.

Furthermore, the rate capability is investigated with a current density from 0.5 to 20 A g^{-1}, as shown in Figure 3d. The Ge-Sn composite exhibits the average specific discharge capacity of 1440, 1200, 1010, 890, 830, 777, 731, 670, and 640 mAh g^{-1} at a current density of 0.5, 1.0, 2.0, 3.0 5.0, 7.0, 10.0, 15.0, and 20.0 A g^{-1}, respectively. Even at 20 A g^{-1}, the specific capacity is over 640 mAh g^{-1} that is far higher than that of the theoretical capacity of commercial graphite anode. After cycling at high current density, a reversible capacity as high as 1180 mAh g^{-1} could be restored as the current density returned back to 0.5 A g^{-1}, indicating a good rate capability. It should be noted that the CE maintains above 97% at

different current density, which is important for practical application.

The long-term cycling stability at higher current density is also evaluated at 3.0 A g^{-1}, as exhibited in Figure 3e. It should be mentioned first that the Ge-Sn based half-cells are tested at 0.3 A g^{-1} for the first two cycles to activate the electrode sufficiently. [26] Impressively, the Ge-Sn composite displays a discharge capacity of 890 mAh g^{-1} even after 1700 cycles. Before 150th cycle, the capacity decays obviously to 950 mAh g^{-1}. But, from 150th cycle forward, only a fading rate of 0.004% is detected, indicating unexceptionable long-term cycling stability. Compared with previously reported results in Ge-Sn based anodes as presented in Table S1. As one can see, the Ge-Sn anode fabricated in this work shows the longest cycling stability up to 1700 cycles with high reversible capacity and current density, and appreciable rate capability.

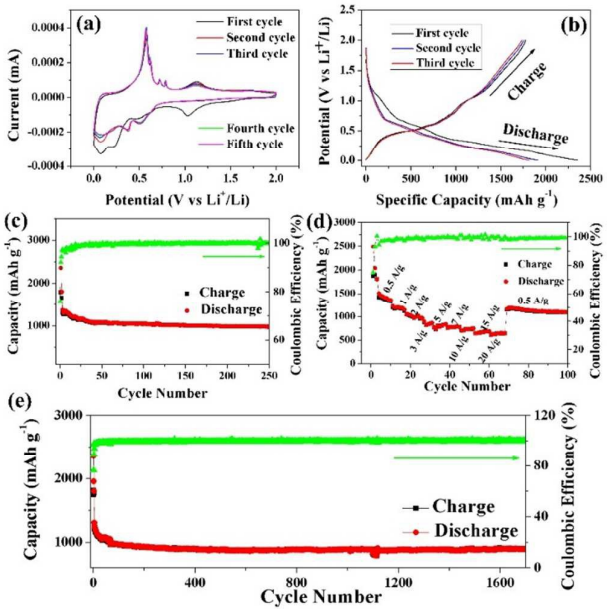

Figure 3. (a) The cyclic voltammogram and (b) the voltage-capacity plots of the as-prepared Ge-Sn composite. The discharge/charge cycling performance of the Ge-Sn composite(c) at a current density of 0.5 A g^{-1}, (d) rate capability with a current density ranging from 0.5 to 20 A g^{-1}, and (e) at a current density of 3 A g^{-1}.

A full cell consisting of a Ge-Sn anode and a commercial $LiCoO_2$ cathode was assembled and tested. The capacity of the cathode was about 10% higher with respect to the anode so that the capacity of the cell was anode limited. The anode was prelithiated using lithium metal in a half-cell to form the stable SEI layer prior to capacity matching with the cathode. [27] The discharge/charge current density and the specific capacity are calculated based on the weight of Ge-Sn. Figure 4a depicts the typical charge-discharge voltage curves with a voltage window from 2.5 to 4.2 V. As one can see, the main discharge and charge potential is at around 3.6 V. The cycling behavior and the corresponding CE at a current density of 140 mA g^{-1} is exhibited Figure 4b. The cell delivers an initial charge capacity of 878 mAh g^{-1} with an initial CE of 84%, and the capacity retains over 94% after 22 cycles. At high current density of 500 mA g^{-1}, the full cell exhibits a reversible capacity of 387 mAh g^{-1} after 120 cycles (Figure S7). To further improve the performances, balancing of the anode and cathode capacity and tuning the voltage window is necessary in the future work.

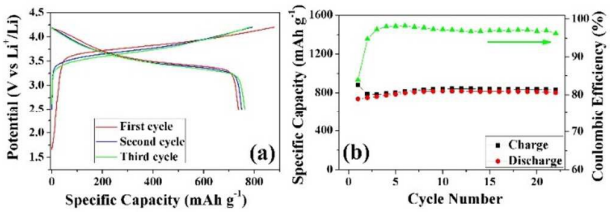

Figure 4. (a) Charge-discharge profile (b) Charge/discharge capacity at a current density of 140 mA g^{-1} and the corresponding coulombic efficiency of the full cell consists of a Ge-Sn anode and a $LiCoO_2$ cathode.

The ex situ XRD patterns, SEM and EDX mapping pictures was exhibited in Figure S8, 9. As we can see, the integrity of the electrode is maintained well even after long term cycling. Notably, the Ge and Sn components are converted from crystalline into amorphous phase, but, still distributed uniformly after cycling. The impressive electrochemical performance of the Ge-Sn binary composite such as long-term cycling stability and fine rate capability may be attributed to the porous hierarchical structure and the synergistic effects. The stepwise Li ion insertion mechanism of Ge and Sn could avoid the rapid volume changes during lithiation/delithition, maintaining the integrity of the active materials. The fine electrical and ionic conductivity of Sn and Ge is significant for enhancing the fast electron and ion diffusion, facilitating the rate capability. What's more, the hierarchical structure assembled with nanoparticles are favorable for further accommodating the volume change, and the porous structure would shorten the Li-ion transfer path.

In summary, the typical metathesis reaction between solid Mg_2Ge and liquid $SnCl_4$ is introduced to prepare Ge-Sn binary composite. The obtained composite shows porous hierarchical structure composed of interconnected nanoparticles in which Ge and Sn are uniformly distributed, associated with a tap density of 2.3 g cm^{-3}. As anode for LIBs, the as-prepared Ge-Sn composite displays a reversible capacity of 980 mAh g^{-1} at 0.5 A g^{-1} after 250 cycles, 890 mAh g^{-1} at 3 A g^{-1} over 1700 cycles, and superior rate capability. When coupled with a commercial $LiCoO_2$ cathode, a 3.6 V full lithium ion battery with a capacity of 830 mAh g^{-1} is obtained. It is demonstrated that the fine electrochemical performance may be attributed be the porous hierarchical structure and the synergistic effect of the contained Ge and Sn. Remarkably, this type of metathesis reaction are also demonstrated to be applicable for fabricating other complex composite such as Si-C and Si-Sn composite.

Notes and references

1 C. Wu, J. Maier, Y. Yu, *Adv. Funct. Mater.*, 2015, **25**, 3488-3496; D. T. Ngo, R. S. Kalubarme, H.T. T. Le, J. G. Fisher, C-N.

Park, Il-Doo Kim and C-J. Park, *Adv. Funct. Mater.,* 2014, **24**, 5219-5224; C. Chae, H-J. Noh, J. K. Lee, B. Scrosati, and Y-K.Sun, *Adv. Funct. Mater.,* 2015, **25**, 3488-3496; X. Li, Z. Yang, Y. Fu, L. Qiao, D. Li, H. Yue, D. He, *ACS Nano,*2015, **9**, 1858-1867; N. Lin, Y. Han, L. Wang, J. Zhou, J. Zhou, Y. Zhu, Y. Qian, *Angew. Chem. Int. Ed*., 2015, **54**, 3822-3825.

2 M. I. Bodnarchuk, K. V. Kravchyk, F. Krumeich, S. T. Wang, M. V. Kovalenko, *ACS Nano,* 2014, **8**, 2360-2368.

3 Y. J. Cho, C. H. Kim, H. SoonIm, Y. Myung, H. S. Kim, S. H. Back, Y. R. Lim, C. S. Jung, D. M. Jang, J. Park, S. H. Lim, E. H. Cha, K. Y. Bae, M. S. Song, Won. Cho, *Phys. Chem. Chem. Phys.,* 2013, **15**, 11691-11695.

4 W. J. Zhang, *J. Power Sources,* 2011, **196**, 877-885; M. N. Obrovacand, V. L. Chevrier, *Chem. Rev.,* 2014, **114**, 11444-11502;

5 H. Kim, Y. Son, C. Park, M-J. Lee, M. Hong, J. Kim, M. Lee, J. Cho, H. C. Choi, *Nano Lett.,* 2015, ***15***, 4135-4142.

6 T. Song, H. Y. Cheng, K. Town, H. Park, Robert W. Black, S. Lee, W. Park, Y. G. Huang, J. A. Rogers, L. F. Nazar, U. Paik, *Adv. Funct. Mater*., 2014, **24**, 1458-1464.

7 J. Li, C. Yue, Y. J. Yu, Y-S. Chui, J. Yin, Z. G. Wu, C. D. Wang, Y. S. Zang, W. Lin, J. T. Li, S. T. Wu, Q. H. Wu, *J. Mater. Chem. A,* 2013, **1**, 14344-14349.

8 T. Song, H. Y. Cheng, H. Choi, J-H. Lee, H. Han, D. H. Lee, D. S. Yoo, M-S. Kwon, J-M. Choi, S. G. Doo, H Chang, J. L. Xiao, Y. G. Huang, W. Park, Y-C. Chung, H. S. Kim, J. A. Rogers, U. Paik, *ACS Nano,* 2012, **6**, 303-309.

9 J. Z. Wang, N. Du, Z. Q. Song, H. Wu, H. Zhang, D. R. Yang, *Journal of Power Sources,* 2013, **229**, 185-189.

10 Y. J. Yu, C. Yue, S. B. Sun, W. Lin, H. Su, B. B. Xu, J. T. Li, S. T. Wu, J. Li, J. Y. Kang, *ACS Appl. Mater. Interfaces,* 2014, **6**, 5884-5890.

11 P. R. Abel, A. M. Chockla, Y-M Lin, V. C. Holmberg, J. T. Harris, B. A. Korgel, A. Heller, C. B. Mullins, *ACS nano,* 2013, **7**, 2249-2257.

12 W. Luo, X. F. Wang, C. Meyers, N. Wannenmacher, W. Sirisaksoontorn, M. M. Lerner, X. L. Ji, *Sci. Rep.,* 2015, **3**, 2222.

13 H. Lee, J. Cho, *Nano Lett.,* 2007, **7**, 2638-2641.

14 J. Cho, *Electrochim. Acta,* 2008, **54**, 461-466.

15 Y. Kwon, J. Cho, *Chem. Commun.*, 2008, 1109-1111; X. Y. Wang, Z. X. Wen, Y. Liu, X. W. Wu, *Electrochim. Acta,* 2009, **54**, 4662-4667.

16 D. Duveau, B. Fraisse, F. Cunin, L. Monconduit, *Chem. Mater.,* 2015, ***27***, 3226-3233.

17 S. F. Fan, L. Y. Lim, Y. Y. Tay, S. S. Pramana, X. H. Rui, M. K. Samani, Q. Yan, B. K. Tay, M. F. Toney, H. H. Hng, *J. Mater. Chem. A,* 2013, **1**, 14577-14585.

18 C. S. Yang, R. A. Bley, S. M. Kauzlarich, H. W. H. Lee, G. R. Delgado, J. *Am. Chem. Soc.,* 1999, **121**, 5191-5195; R. Epur, L. Minardi, M. K. Datta, S. J. Chung and P. N. Kumta, *J. Solid State Chem.,* 2013, **208**, 93-98; K. A. Pettigrew, Q. Liu, P. P. Power and S. M. Kauzlarich, *Chem. Mater.,* 2003, **15**, 4005-4011.

19 L. B. Wang, N. Lin, J. B. Zhou, Y. C. Zhu and Y. T. Qian, *Chem. Commun.,* 2015, **51**, 2345- 2348.

20 D. Sun, A. E. Riley, A. J. Cadby, E. K. Richman, S. D. Korlann, S. H. Tolbert, *Nature,* 2006, **44**, 1126-1130; G. S. Armatas, M. G. Kanatzidis, *Nature,* 2006, **44**, 1122-1126.

21 N. Lin, L. Wang, J. Zhou, J. Zhou, Y. Han, Y. Zhu, Y. Qian, C. Cao, *J. Mater. Chem. A,* 2015, **3**, 11199-11202.

22 M. Oehme, K. Kostecki, M. Schmid, F. Oliveira, E. Kasper, J. Schulze, *Thin Solid Films,* 2014, **557**, 169-172; S. J. Su, B. W. Cheng, C. L. Xue, W. Wang, Q. Cao, H. Y. Xue, W. X. Hu, G. Z. Zhang, Y. H. Zuo, Q. M. Wang, *Opt. Express,* 2011, **19**, 6400-6405.

23 S. F. Li, M. R. Bauer, J. Menendez, J. Kouvetakis, *Appl. Phys. Lett.,* 2004, **84**, 864-869; V.R. D'Costa, J. Tolle, R. Roucka, C.D. Poweleit, J. Kouvetakis, J. Men ´endez, *Solid State Commun.,* 2007, **144**, 240-244.

24 Y. Yue, H. Liang, *J. Power Sources,* 2015, **284**, 435-445.

25 P. R. Abel, M. G. Fields, A. Heller, C. B. Mullins, *ACS Appl. Mater. Interfaces,* 2014, **6**, 15860-15867.

26 N. Lin, J. B. Zhou, L. B. Wang, Y. C. Zhu and Y. T. Qian, *ACS Appl. Mater. Interfaces*, 2015, **7**, 409-414.

27 I. H. Son, J. H. Park, S. Kwon, S. Park, M. H. Rummeli, A. Bachmatiuk, H. J. Song, J. Ku, J. W. Choi, J. Choi, S-G. Doo, H. Chan, *Nat. Commun.,* 2015, **6**, 7393-7400.

